

# Effect of Ni/MoS<sub>2</sub> Addition on Microstructure and Properties of Supersonic Plasma-Sprayed Ni-Based Composite Coatings

Xinsheng WANG<sup>1,2</sup>, Wenbin HE<sup>1\*</sup>, Junjian HOU<sup>1</sup>, Kun LIU<sup>1</sup>, Xihao YAN<sup>1</sup>

<sup>1</sup> Hennan Key Laboratory of Intelligent Manufacturing of Mechanical Equipment, Zhengzhou University of Light Industry, Zhengzhou, 430002, China

<sup>2</sup> Henan Engineering Research Center of New Energy Vehicle Light Weight Design and Manufacturing, Zhengzhou, 430002, China

**crossref** <http://dx.doi.org/10.5755/j02.ms.29299>

Received 18 June 2021; accepted 09 September 2021

Abnormal tool wear is a significant problem encountered in machining. MoS<sub>2</sub> has the function of friction reduction; thus, to mitigate friction, two Ni-based coatings, Ni60 and Ni60 + 15 wt.% Ni/MoS<sub>2</sub>, were obtained on tungsten steel using supersonic plasma technology. The microstructure, phase structure, microhardness, fatigue properties, and friction and wear properties of the two coatings were characterized. The results show that the two plasma-sprayed Ni-based coatings have desirable structures. The addition of Ni-coated MoS<sub>2</sub> can effectively improve the hardness of the coatings, with values reaching as high as 735 HV. The speed of rotation of the friction ball was set as 200 r/min, and the cutting force was 201.6 N. The fatigue performance as well as the friction and wear performance of the coating are simulated using ANSYS. The fatigue performance is improved by 12.6 % after adding 15 wt.% Ni/MoS<sub>2</sub>, and the friction system of the coating becomes stable after 25 min of contact. The addition of 15 wt.% Ni/MoS<sub>2</sub> can effectively improve the performance of the tool material.

**Keywords:** supersonic plasma technology, Ni coating, hardness, fatigue properties, friction, wear.

## 1. INTRODUCTION

The rapid pace of development in aerospace, defence, energy, automobile, and other cutting-edge industries has made material property requirements more and more stringent, resulting in the development of several new and improved materials. As critical components in fabrication industries, cutting tools require special attention, especially since the tool-chip contact surface is subjected to severe friction. As the friction on the tool surface increases, the cutting temperature also increases, making cutting difficult [1].

High-temperature wear-resistant coatings on the surface of tool parts is an effective way to reduce the high-temperature wear of tool chips [2]. At present, iron-based and nickel-based composite coatings have excellent wear resistance, but their characteristics limit their application. For example, when working under high-temperature or corrosive environments, or when subjected to heavy loads, the friction surface cannot form an effective lubricating layer, and the wear is severe [3–5]. Coated tools are a class of tools made of high-hardness steel whose surface is coated with refractory metal or nonmetal compounds having good wear resistance. Coating materials generally do not react with the substrate material, have high hardness, high wear resistance, high chemical stability, good heat and oxidation resistance, and low friction coefficient. Such materials, including TiC, TiN, TiAlN coating materials, can adhere to the substrate firmly [6–8]. There are four kinds of coated tools: coated high-speed steel tools, coated cemented carbide tools, and coated tools on ceramic and

super-hard material (diamond or cubic boron nitride) blades. MoS<sub>2</sub> is a transition metal compound with low cost and stable chemical properties. The atoms in the molecular layers are held together by van der Waals forces and subject to small shear stresses, namely, fracture and slip. It has a layered structure with a low friction coefficient, good lubricity, and high thermal stability, which can provide effective lubrication during low temperature friction [9–11].

As a self-soluble alloy with a low melting point, good fluidity, high hardness, and stable microstructure and properties, Ni60 powder is often used to prepare heat-resistant, corrosion-resistant, oxidation-resistant, and high-temperature wear-resistant coatings, and is commonly used in nickel-based alloy powder [12].

In this experiment, NiCrBSi (Ni60) powder and Ni-coated MoS<sub>2</sub>/Ni60(Ni60-NM) powder were used as raw materials to prepare composite coatings, and the microstructure and properties were analyzed.

## 2. EXPERIMENTAL

### 2.1. Spraying material

Tungsten steel having a particular composition (mass fraction, %: 5.5–6.75 W; 4.5–5.5 Mo; 3.8–4.4 Cr; 0.8–0.9 C; 1.75–2.2 V; 0.2–0.45 Si; 0.15–0.4 Mn, the rest is Fe) was used as substrate. The material was provided by Shaanxi Best Mold Co., LTD. Fig. 1 shows the tungsten steel spraying substrate. The chemical composition of Ni60 was (mass fraction, %: 17–18 Cr; 4–5 Fe; 4–4.5 Si; 0.7–1.1 C, 2.7–3.5 B, the rest is Ni). Ni-coated MoS<sub>2</sub> powder (Ni/MoS<sub>2</sub>) with a particle size of 15–45 μm. Ni60 and Ni60 + 15 wt.% Ni/MoS<sub>2</sub> (Ni60-NM) were used as spray powder and mechanically mixed

\* Corresponding author. Tel.: +086-0371-86601650; fax: +086-0371-86601652. E-mail address: [hwb@zzuli.edu.cn](mailto:hwb@zzuli.edu.cn) (W. He)

powder, respectively [13, 14], which are supplied by Haotian Nano Technology (Shanghai) Co., LTD.

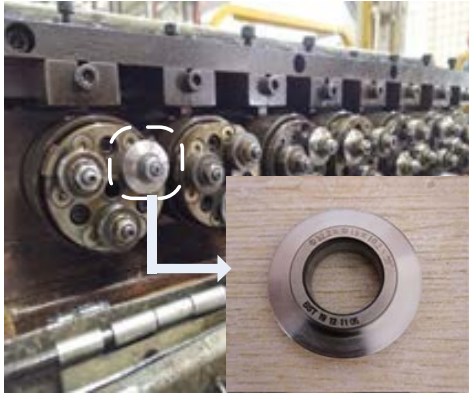


**Fig. 1.** Tool materials tested

Fig. 2 shows the micro scanning images of the two powders. XRD was also used to analyze the phase of the Ni60 and Ni60-NM powders. Ni60 powder contains Ni, Cr<sub>23</sub>C<sub>6</sub>, NiSi, Ni<sub>3</sub>Si<sub>2</sub>, and NiB<sub>12</sub> phases [12], the Ni60-NM powder contains Ni and MoS<sub>2</sub> phases.

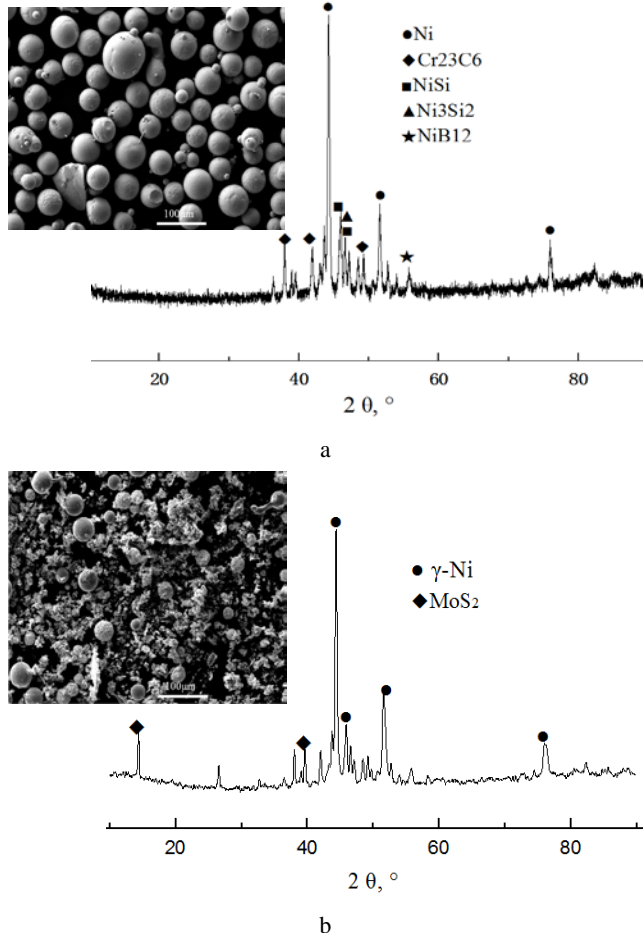


**Fig. 2.** Microscanning images of the two powders. a–Ni60 powder; b–Ni60-NM powder

## 2.2. Spraying technology

HDV-8000 supersonic plasma spraying equipment (Zhengzhou Lijia spraying Co., Ltd.) was used to prepare the composite coating. The Ni60 and Ni60-NM coating

materials were prepared. Table 1 shows the parameters used in the process, including plasma spraying [3].

## 2.3. Structure characterization and performance analysis

The phase structure of the coating surface after spraying was analyzed using polycrystalline X-ray diffraction (XRD, SHIMADZU XRD 7000). The microstructure of the coating was characterized by the scanning electron microscope (SEM, HITACHI-S 3400). The hardness of the coating was measured on the digital microhardness tester (Hv, HXD-1000). The test time was 15 s and the loading force was 0.3 kg. Three measurements at positions from the center to the edge of the coating were measured and the average value was calculated.

**Table 1.** Plasma spraying technique parameters

| Number of Coating                    | Parameter |
|--------------------------------------|-----------|
| Spraying current, A                  | 350       |
| Spraying voltage, V                  | 110       |
| Argon gas flow, m <sup>3</sup> /h    | 3.7       |
| Hydrogen gas flow, m <sup>3</sup> /h | 0.2       |
| Spraying distance, mm                | 120       |
| Powder feed rate, g/min              | 36        |
| Nitrogen gas flow, m <sup>3</sup> /h | 0.6       |
| Thickness of coating, μm             | 300       |

ANSYS was used to simulate the friction and wear. The parameters of the Ni60 coating were set as follows: elastic modulus 218 GPa, density 8.3 g/cm<sup>3</sup>, Poisson's ratio 3.1, ultimate compressive strength 2100 MPa. The material parameters of the Ni60-NM tool were set as follows: elastic modulus 223 GPa, density 8.7 g/cm<sup>3</sup>, ultimate compressive strength 2280 MPa, and Poisson's ratio 0.35.

## 3. RESULTS AND DISCUSSION

### 3.1. Microstructure and XRD analysis of coating

It can be seen from the surface of the sample after spraying shown in Fig. 3 a that the microstructure of Ni60 was relatively uniform, with fewer pores and holes. The spraying is relatively dense, with an obvious layered structure and few high temperature oxides and inclusions. However, The surface structure is relatively dense, and the spraying effect was good.

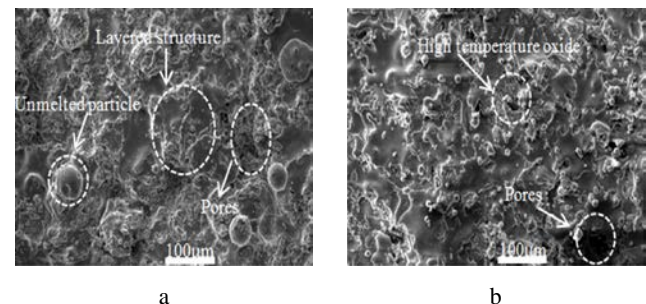


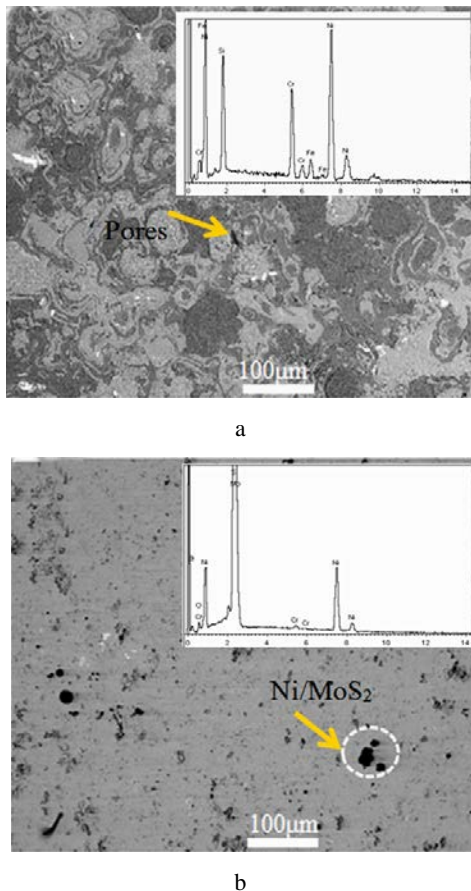
**Fig. 3.** Surface morphology of spraying samples: a–Ni60; b–Ni60-NM

Despite the good fusibility of Ni60 in high-temperature spraying and the good combination of Ni60 material and metal structure, there is the presence of some unmelted particles. In Fig. 3 b, there are many pores and

holes on the surface of the Ni60-NM coating, and the uniformity and compactness of the coating are not as good as that of Ni60 surface spraying. At the same time, there are many high-temperature oxides in the coating. This is because there are gas barriers and foreign impurities during the formation of coating materials, which deteriorate the spraying compactness and spraying effect.

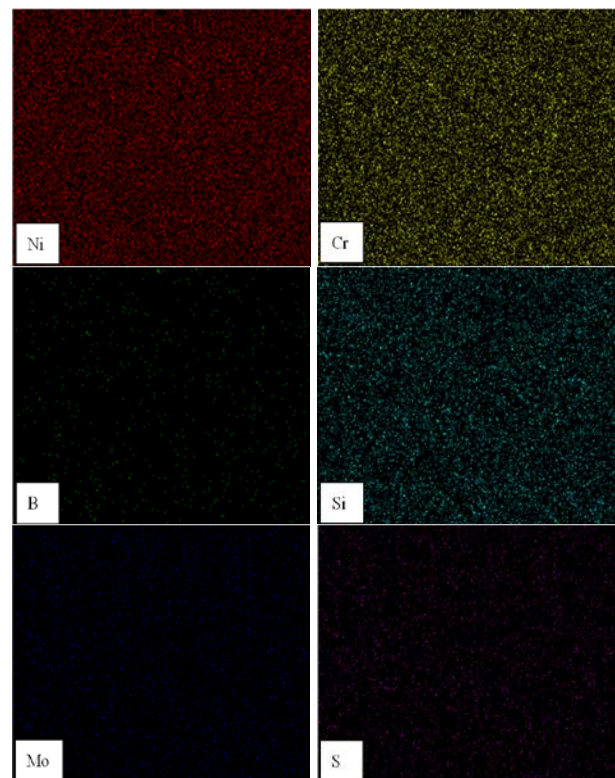
The analysis suggests that the appearance of pores and holes may be due to the uneven melting of the spraying powder during the spraying process, uneven diffusion of the spray gun pressure, and hindrance caused by the gas to the combination of a small number of spraying materials during the spraying process. The layered structure may be due to the uniform diffusion of powder in the spraying process and the formation of a layered structure after repeated spraying. The unfused materials may result from uneven or deficient heating during spraying. The appearance of high-temperature oxides may be due to the presence of external impurities [12]. If the spraying is not uniform or the surface roughness of the base material is too large, cracks will appear.

Fig. 4 shows the scanned image of the two coating materials after polishing (200-1000 mesh number sandpaper) and acid corrosion (HCl:HNO<sub>3</sub> = 3:1). Both the coatings have a typical layered structure formed by the continuous collision of droplets and the spreading and accumulation of flat particles. The interface between the layers is clear, and the pores are mainly generated at the interface.



**Fig. 4.** Microscopic morphology picture of the sample: a–Ni60; b–Ni60-NM

The high-speed impact of semi-molten coating material on the substrate is accompanied by strong plastic deformation and rapid solidification, and small pores may appear in the thermal spray coating. When MoS<sub>2</sub> was added into a Ni-based coating, a black phase appeared in the coating, and its content increased with the increase in the Ni/MoS<sub>2</sub> content. EDS analysis of the black phase in the coating shows it is mainly composed of Ni, Mo, and S, and so, it can be qualitatively determined that the black phase is Ni/MoS<sub>2</sub>. The best way to protect the coating was to ensure a good binding force between the coating and the substrate [15]. The elemental distribution images of the coatings indicate the distribution of various elements on the surface of the coatings. Fig. 5 shows the distribution of elements on the surface of the Ni60-NM coatings.



**Fig. 5.** Distribution of elements of the Ni60-NM coatings

In Fig. 5, the distribution of elements is relatively uniform. The material mainly contains Ni, Cr, B, Si, Mo and S. Fig. 6 shows the XRD phase structure of the Ni60-NM coatings, and mainly shows the presence of Ni, Ni<sub>3</sub>Si<sub>2</sub>, Ni<sub>2</sub>Cr<sub>13</sub>, MoS<sub>2</sub>.

### 3.2. Microhardness analysis

Fig. 7 is the microhardness diagram of the spray coating. The surface hardness is tested at the positions shown in the figure, each sample is tested for 5 hardness values, and the average value is obtained. The microhardness of Ni60 was 715 HV and the hardness of the coating after the addition of Ni/15 MoS<sub>2</sub> was 735 HV, indicating an increase of 2.5 %. The addition of Ni-coated MoS<sub>2</sub> particles improves the microhardness of the coating, which may be due to the decrease in porosity and the denser coating. This is because Ni60-NM coating is the specimen after polishing treatment, while Fig. 3 is the

specimen after spraying, which is also the difference between them.

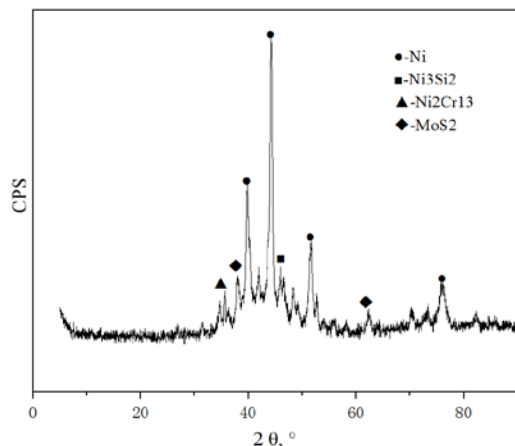


Fig. 6. XRD pattern of the Ni60-NM coating

The results show that the porosity of MoS<sub>2</sub> as the lubricating phase is reduced and the coating was more compact. The hardness of the coating was improved. The reason for the increase in microhardness is that, on the one hand, the addition of MoS<sub>2</sub> with higher hardness increases the microhardness of the coating, and on the other hand, the coating is denser due to the decrease in the porosity of the coating, which leads to a gradual improvement in the microhardness of the coating [16]. However, in the MoS<sub>2</sub>/Nb coating, the maximum hardness after adding 15 % MoS<sub>2</sub> is 336 HV, which is about half of that in this paper, MoS<sub>2</sub>/Nb shows a crystalline orientation and dense structure, and this phase has better lubrication performance in a wet environment, There was also higher hardness [17].

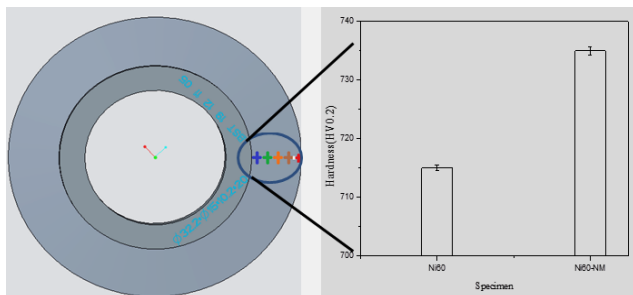


Fig. 7. The average hardness of spray samples

### 3.3. Fatigue performance analysis

ANSYS is used to simulate and analyze the stress in the tool coating material. The center rotating surface of the tool is assumed fixed, and the force involved was mainly the cutting force. When the cutting force was 201.6 N, the maximum deflection is obtained and the maximum deformation was  $1.9 \times 10^{-6}$  mm; the cutting stress in X, Y, and Z directions of the Ni60 and Ni60-NM coatings are shown in Table 2, and the simulated stress plot is shown in Fig. 8.

Table 2. The parameters of the sample of X, Y, Z direction

| Sample  | X, MPa   | Y, MPa   | Z, MPa   |
|---------|----------|----------|----------|
| Ni60    | -0.31002 | -0.29284 | -0.45631 |
| Ni60-NM | -0.29477 | -0.22801 | -0.43427 |

The contact stress of the Ni60-NM coating in the X, Y, and Z directions is increased; the higher the contact stress and strain of the tool material, the lower the hardness of the material, which is consistent with the change in the hardness of the coating.

Table 3 shows the number of fatigue cycles predicted before tool cutting failure.

Table 3. Fatigue cycles predicted before tools cutting failure

| Sample  | Fatigue life, circle |
|---------|----------------------|
| Ni60    | 210622               |
| Ni60-NM | 237242               |

From the number of fatigue cycles, it can be seen that the number of cycles associated with the Ni60-NM coating is higher than that of Ni60 coating. According to the analysis results of tool modeling, the fatigue life of the Ni60-NM coating tool was 12.6 % higher than that of the Ni60 coating tool, which was also consistent with the change in coating hardness.

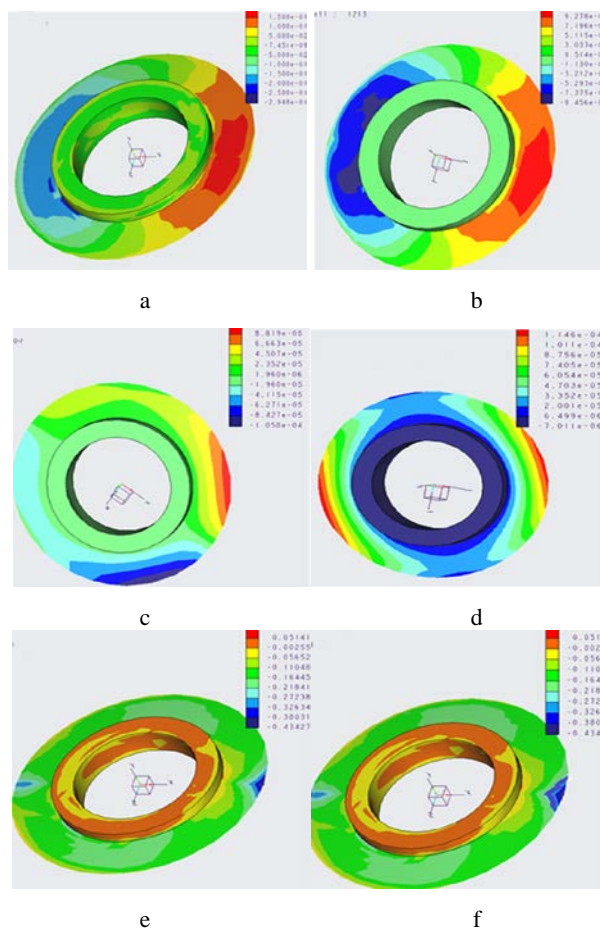


Fig. 8. Cutting stress in X, Y, Z directions of sample: a–X; c–Y; e–Z Ni60; b–X; d–Y; f–Z Ni60-NM

### 3.4. Analysis of friction and wear performance

The speed of rotation of the friction ball was set as 200 r/min. The force analyses of the Ni60-coated tool and Ni60-NM-coated tool are carried out respectively, and the force condition was the same as that of stress analysis:

$$\mu = F/N, \quad (1)$$

where  $F$  is the friction force;  $N$  is the vertical pressure, and the main cutting force 201.6 N. The friction coefficient is obtained from the simulation, and the average friction coefficient of the sample at different times is shown in Fig. 9. It can be seen from this figure that the addition of NM reduces the friction coefficient, and that the addition of NM has a low friction coefficient and excellent scratch resistance under sliding friction. The reduction of friction coefficient may be due to the formation of a  $\text{MoO}_2$  film on the surface, which can prevent metal-to-metal contact and maintain a low friction coefficient. The increase in friction coefficient occurs at the friction completion stage, which may be because the toughness of Ni enhances the bonding strength between the layers and the compactness of layers, which produces greater resistance to friction during the friction process, reduces the delamination degree during continuous sliding contact, and increases the friction coefficient in Ni- $\text{MoS}_2$  coating.

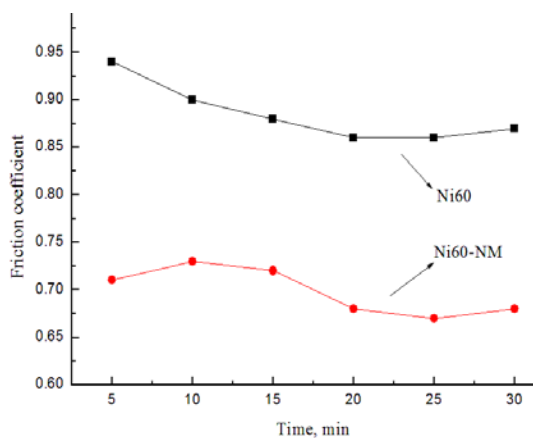


**Fig. 9.** Average friction coefficient of the sample at different times

This shows that the compound during the friction process of the coating had the function of  $\text{MoS}_2$  lubricating. It plays a good role in antifriction lubrication [18].

#### 4. CONCLUSIONS

Ni60-NM coating has a good structure, and the hardness of the coating is 2.5 % higher than that of the Ni60 coating. The fatigue resistance of the Ni60-NM coating is increased by 12.6 % compared to the Ni60 coating. In the ANSYS simulation, the friction coefficient of the Ni60-NM coating is reduced to 0.67 after 25 minutes of motion, which indicates a better performance than the Ni60 coating. Thus, the addition of Ni/ $\text{MoS}_2$  effectively improves the performance of the tool material.

#### Acknowledgments

This work is financially supported by the National Science Foundation of China (No. 51775554, U2004169) and Natural Science Foundation of Henan Province (No. 202300410505). Foundation of Key Laboratory of National Defense Science and Technology (No. 6142005200302) is gratefully acknowledged. Training program for young backbone teachers in colleges and universities of Henan province (2019GGJS130) and key scientific and technological project of Henan Province

(202102210290). The authors thank the editor and the anonymous reviewers for their helpful comments and suggestions.

#### REFERENCES

- Vinay, V., Akhil, K., Ramesh, M.R., Chakradhar, D.** Investigation on the Performance of AlCrN and AlTiN Coated Cemented Carbide Inserts during end Milling of Maraging Steel under Dry, Wet and Cryogenic Environments *Journal of Manufacturing Processes* 43 2019: pp. 136–144. <https://doi.org/10.1016/j.jmapro.2019.05.021>
- Wang, X.S., Xing, Z.G., Hou, J.J., Liu, K.** Influence of Oxidized Ceramics on the Tribological Properties of Ni60/WC Composite Coatings *Journal of Physics Communications* 4 2020: pp. 035001–035011. <https://doi.org/10.1088/2399-6528/ab7617>
- Wang, X.S., Xing, Z.G.** Preparation and Properties of Composite Nanoceramic NiCrBSi-TiO<sub>2</sub>/WC(Co) Coatings *Coatings* 10 (9) 2020: pp. 868–879. <https://doi.org/10.3390/coatings10090868>
- Zhang, J.F., Liu, M., Song, J.B., Deng, C.M., Deng, C.G.** Microstructure and Corrosion Behavior of Fe-based Amorphous Coating Prepared by HVOF *Journal of Alloys and Compounds* 721 2017: pp. 506–511. <https://doi.org/10.1016/j.jallcom.2017.06.046>
- Guével, Y.L., Grégoire, B., Cristóbal, M.J., Feugas, X., Oudriss, A., Pedraza, F.** Dissolution and Passivation of Aluminide Coatings on Model and Ni-based Super Alloy *Surface and Coatings Technology* 357 2019: pp. 1037–1047. <https://doi.org/10.1016/j.surfcoat.2018.10.090>
- Zhang, F.Y., Li, C., Yan, S., He, J.N., Liu, B.X., Yin, F.X.** Microstructure and Tribological Properties of Plasma Sprayed TiCN-Mo Based Composite Coatings *Applied Surface Science* 464 2019: pp. 88–98. <https://doi.org/10.1016/j.apsusc.2018.09.063>
- Chen, J.B., Dong, Y.C., Wan, L.N., Yang, Y.** Effect of Induction Remelting on the Microstructure and Properties of in Situ TiN-reinforced NiCrBSi Composite Coatings *Surface & Coatings Technology* 340 2018: pp. 159–166. <https://doi.org/10.1016/j.surfcoat.2018.02.024>
- Li, B.W., Liu, Q., Chen, M.H., Niu, Y.S., Zhu, S.L., Wang, F.H.** Ru-induced Microstructural Change in Ion-plated TiN Coating and its Tribological Properties *Surface and Coatings Technology* 354 2018: pp. 175–183. <https://doi.org/10.1016/j.surfcoat.2018.09.028>
- Rezapoor, M., Razavi, M., Zakeri, M., Rahimipour, M.R., Nikzad, L.** Fabrication of Functionally Graded Fe-TiC Wear Resistant Coating on CK45 Steel Substrate by Plasma Spray and Evaluation of Mechanical Properties *Ceramics International* 44 2018: pp. 22378–22386. <https://doi.org/10.1016/j.ceramint.2018.09.001>
- Hu, S.H., Muhammad, M.F., Wang, M.Z., Ma, R.N.** Corrosion Resistance Performance of Nano- $\text{MoS}_2$ -Containing Zinc Phosphate Coating on Q235 Steel *Materials Letters* 265 2020: pp. 127256–127260. <https://doi.org/10.1016/j.matlet.2019.127256>
- Gülden, A., Abdurrahman, A., Hüseyin, Ç.** The Effect of 2D- $\text{MoS}_2$  Doped Polypyrrole Coatings on Brass Corrosion *Journal of Molecular Structure* 1203 2020: pp. 127318–127323. <https://doi.org/10.1016/j.molstruc.2019.127318>

12. **Wang, X.S., Xing, Z.G., Liu, Y.P., Hou, J.J., Liu, K.** Composite Ceramic-Ni60 Coating Fabricated Via Supersonic Plasma *Chinese Journal of Physics* 61 2019: pp. 72–79.  
<https://doi.org/10.1016/j.cjph.2019.08.012>
13. **Maharana, H.S., Mondal, K.** Manifestation of Hall-Petch Breakdown in Nanocrystalline Electrodeposited Ni-MoS<sub>2</sub> Coating and its Structure Dependent Wear Resistance Behavior *Surface and Coatings Technology* 410 2021: pp. 126950–126961.  
<https://doi.org/10.1016/j.surfcoat.2021.126950>
14. **Wang, Q., Li, X., Niu, W.** Effect of MoS<sub>2</sub> Content on Microstructure and Properties of Supersonic Plasma Sprayed Fe-based Composite Coatings *Surface and Coatings Technology* 391 2020: pp. 125699–125718.  
<https://doi.org/10.1016/j.surfcoat.2020.125699>
15. **Hikmet, C., Ozan, C.A., Ihsan, E.** Structure and Adhesion Properties of TiNi/MoS<sub>2</sub> Coatings *Ceramics International* 47 2021: pp. 14033–14040.  
<https://doi.org/10.1016/j.ceramint.2021.01.272>
16. **Vcx, Y.J., He, Z., Wang, Y.** Microstructure and Wear Resistance of Plasma-sprayed Molybdenum Coating Reinforced by MoSi<sub>2</sub> Particles *Journal of Thermal Spray Technology* 25 (7) 2016: pp. 1322–1329.  
<https://doi.org/10.1007/s11666-016-0440-6>
17. **Gaur, A., Sahoo, S., Ahmadi, M.S.** Surface Energy Engineering for Tunable Wettability through Controlled Synthesis of MoS<sub>2</sub> *Nano Letters* 14 (8) 2014: pp. 4314–4321.  
<https://doi.org/10.1021/nl501106v>
18. **Ren, S., Li, H., Cui, M.** Functional Regulation of PbTi/MoS<sub>2</sub> Composite Coatings for Environmentally Adaptive Sid Lubrication *Applied Surface Science* 401 2017: pp. 362–372.  
<https://doi.org/10.1016/j.apsusc.2017.01.054>



© Wang et al. 2022 Open Access This article is distributed under the terms of the Creative Commons Attribution 4.0 International License (<http://creativecommons.org/licenses/by/4.0/>), which permits unrestricted use, distribution, and reproduction in any medium, provided you give appropriate credit to the original author(s) and the source, provide a link to the Creative Commons license, and indicate if changes were made.